[1] Yuzhao Wu
[2,*] Feng Liu
[1] Xiaobo Li
[1] Tiantian Cai
[1] Junjian Chen
[1]Ye Kuang
[1]Yuji Wang
[1]Qiaohui Zhang
[3]Yuzhou Ning

Single-End Protection for Flexible DC Distribution Network Based on the Energy Peak-Average Ratio of Fault Current

Abstract: Aiming at the problem that the traditional protection methods of flexible DC distribution network cannot identify faults and protect lines in a very short time. In This paper, a single-end protection for flexible DC distribution network based on energy peak-to-average ratio is proposed. Firstly, the discharge process at the moment of fault occurrence is analyzed theoretically, and the fault characteristics of bipolar short-circuit fault are explored. The physical meaning of energy peak-average ratio is defined, and the limitation of protection of current sudden change and energy peak-average ratio under different fault locations and fault conditions is analyzed. Finally, a fault identification and line protection method of combining current abrupt change and energy peak-average ratio is proposed. The simulation results show that this method achieves accurate fault identification and fast and reliable protection of the full length of the line, and is not affected by fault location, transition resistance and strong noise.

Keywords: Flexible DC distribution network, bipolar short-circuit fault, energy peak-average ratio, fault characteristics

I. INTRODUCTION

With the increasing popularity of distributed power supply and DC load, the flexible DC distribution network with electronic power conversion devices as the core has gradually become a hot research field at home and abroad due to its advantages of low power loss, flexible system configuration and good compatibility with new energy sources [1]. Most of the flexible DC distribution system is bipolar operation, grounding mode is mostly neutral high resistance ground, because of its small damping, low inertia characteristics, in just a few milliseconds, the fault current may soar to thousands to tens of thousands of amperes[2]. Therefore, the protection action of the flexible DC distribution network requires troubleshooting within 6ms. Since the operation time of the existing hybrid DC circuit breaker is about 3ms, the fault identification time should be controlled within 3ms[3], which makes the instantaneous protection method become the focus of flexible DC distribution technology research. The existing protection principles at home and abroad can be divided into single-end protection and double-end protection, among which single-end protection does not need to communicate at both ends, can act quickly, reduce the protection action time, and is widely used in practical projects[4].

Single-end protection can be divided into time-domain information protection and frequency-domain information protection according to data processing methods. The core of time-domain information protection is to use the characteristics of current or voltage amplitude and sudden change to form the criterion. For example, the literature [5] studies the overcurrent protection of DC systems, while the literature [6] discusses the applicability of undervoltage protection in DC systems. The literature[7] and [8] use differential protection for fault identification based on the difference of voltage and current abrupt change in non-fault and fault conditions. The literature [9] and [10] use the current limiting reactor in DC system as the measuring element, and use its voltage or voltage mutation to form the fault criterion. The common limitation of these methods is that they mainly rely on the electrical volume of a single endpoint for protection, and while it is possible to amplify fault characteristics to distinguish between normal and fault states, it is difficult to distinguish between in-and-out faults. In addition, due to the complex transient process after the fault and the distributed capacitance effect of the line, these protection methods are difficult to adjust. In the case of high-resistance faults, these methods cannot meet the requirements of

[1] China Southern Power Grid Digital Grid Research Institute Co., Ltd., Guangzhou, 510555, China
[2] State Key Laboratory of Disaster Prevention and Reduction for Power Grid, Changsha University of Science and Technology, Changsha, 410114, China
[3]China energy construction group Hunan Electric Power Design Institute Co. , Ltd, Changsha, 410076, China
* Corresponding author's e-mail: 1184568215@qq.com

both rapidity and selectivity. These methods are difficult to be applied to the actual engineering situation of DC distribution network.

The Frequency-domain information protection is mainly based on traveling wave theory and frequency domain characteristics of high frequency impedance to form the basis of protection. The literature [11] and [12] studied the method of identifying line faults by detecting the arrival time of the faulty travelling wave head. This method has a rapid response and has been widely used in the main protection of DC transmission and distribution lines. However, this method is difficult to apply to high-resistance fault cases, and requires a high sampling rate, which makes the cost high. In literature [13], a protection strategy based on the voltage mutation quantity was studied based on the difference of fault travel wave characteristics inside and outside the fault post area, but this method was susceptible to noise. The literature [14] and [15] put forward a single terminal protection method of DC distribution network based on curvature. This method takes advantage of the gentle effect of current-limiting reactor on the fault waveform outside the area, and adopts the maximum curvature of the waveform as the basis for distinguishing faults inside and outside the area. However, because this method only uses the sampling point with the largest curvature to judge, it is easy to be affected by sharp noise and lead to misoperation of protection.

The above protection methods generally have problems such as poor noise tolerance, inability to operate effectively in the case of high resistance faults, and inability to protect the full length of the line. In view of the above reasons, it is of great significance to study a protection method that can quickly protect the full length of the line and accurately identify the faults inside and outside the area without adding extra burden to the system.

To solve the above problems, this paper firstly deduces the transient discharge process of bipolar short-circuit fault in flexible DC distribution network, and analyzes the characteristics of bipolar short-circuit fault in flexible DC distribution network. Define the physical meaning of energy peak-average ratio, then analyze the limitations of current abrupt change and energy peak-average ratio with different fault locations and fault distances, reveal the complementarity of current abrupt change and energy peak-to-average ratio, and form a protection method combining current abrupt change and energy peak-to-average ratio to achieve fast and reliable protection of the full length of the line. This method is not affected by fault location, transition resistance and noise interference, and meets the reliability and rapidity requirements of flexible DC distribution network protection.

II ANALYSIS OF BIPOLAR SHORT-CIRCUIT FAULT CHARACTERISTICS OF FLEXIBLE DC DISTRIBUTION NETWORK

A. Flexible DC distribution network model

This paper takes ±10kV multi-terminal circular flexible DC distribution network as the research object, as shown in Fig 1:

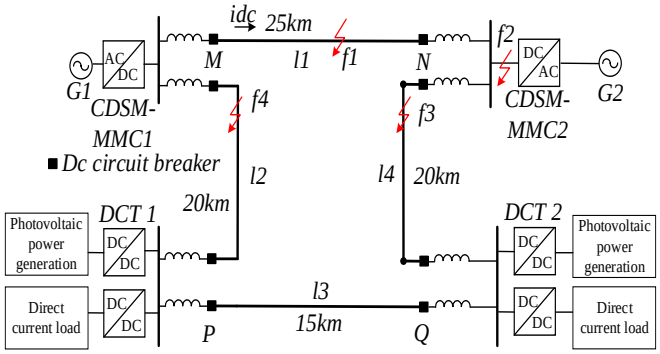

Figure 1: Structure diagram of multi-terminal ring-shaped flexible DC distribution network

As shown in Fig 1, the PV power station is boosted to ±10kV by DCT (DC Transformer) and connected to the ±10kV ring network. After multiple ports connecting ring by MMC (Modular Multilevel Converter) converter equipment and communication system interconnection, AC/DC system parallel operation[16]. The topology of DCT and MMC is as follows.

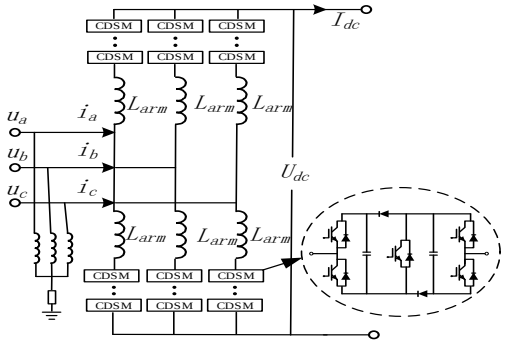

Figure 2: MMC topology structure diagram

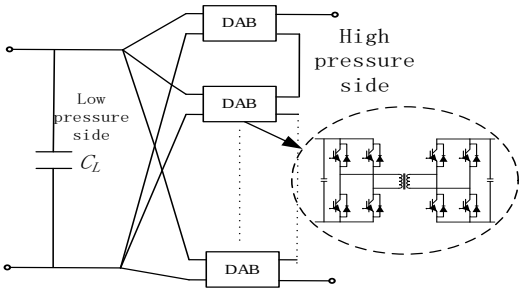

Figure 3: DCT topology structure

As can be seen from Fig 2 and 3, DCT and MMC are composed of multiple Dual Active Bridge (DAB) and Clamp Double Sub-module (CDSM).

B. Analysis of MMC bipolar short-circuit fault characteristics

In the case of bipolar short-circuit fault, the transient fault is mainly divided into fault detection stage and fault isolation stage[17]. When the converter is not locked in the fault detection stage, the fault current is mainly the capacitor discharge current, followed by the AC side feed current[18]. If only the capacitor discharge process is considered, The equivalent capacitance of the converter is calculated according to the principle of constant capacitor energy storage. As shown in formula (1) and (2)[19].

$$\frac{1}{2}C_{CDSM}(\frac{U_{dcN}}{N})^2 \times 6N = \frac{1}{2}C_{eq}U_{dcN}^2 \tag{1}$$

$$C_{eq} = \frac{6C_{\mathrm{CDSM}}}{N} \tag{2}$$

In the above formula, CCDSM is the capacitance value of a single CDSM module, Ceq is the equivalent capacitance of the converter, N is the number of CDSM modules of the bridge arm, and UdcN is the rated voltage between the poles of the DC side.

The equivalent circuit diagram of MMC when fault occurs can be roughly equivalent to the form of capacitor and resistor in series, as shown in Fig 4:

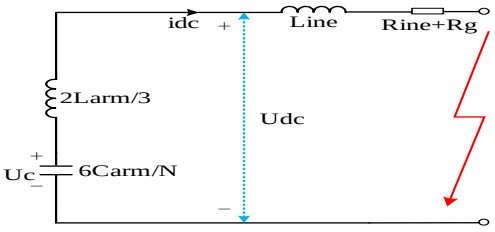

Figure 4: Equival ent circuit diagram of fault detection stage

The equivalent inductance of the fault loop can be obtained from Fig 4 as follows:

$$L_{\mathrm{eq}} = \frac{2L_{arm}}{3} + L_{line} \tag{3}$$

In the above formula, Larm is the inductance of the bridge arm, and Lline is the inductance of the DC line.

Ignoring the on-resistance of the switching device, the equivalent resistance Req in the loop can be obtained as shown in formula (4) :

$$R_{eq} = R_{line} + R_f \tag{4}$$

In the above formula, Rline is the resistance of the DC line, and Rf is the transition resistance when the fault occurs. Assuming that the fault occurs at t=0, the loop differential formula and boundary conditions after the fault are shown in formulas (5) and (6) :

$$L_{eq}C_{eq}\frac{d^2u_C}{dt^2} + L_{eq}C_{eq}\frac{du_C}{dt} + u_C = 0 \tag{5}$$

$$\begin{cases} u_c(0_+) = u_c(0_-) = U_{dc0} = U_{dcN} \\ i_{dc}(0_+) = i_{dc}(0_-) = I_0 \end{cases} \tag{6}$$

In above formulas, Udc0 is the instantaneous voltage value at the protection installation place when the fault occurs, I0 is the instantaneous current value at the protection installation place when the fault occurs, and Idc is the DC current value measured at the protection installation place.

Since the Req of the actual DC distribution network is generally much smaller than $2\sqrt{NL_{eq}/C_0}$ [20], this process can be equivalent to the second-order discharge process, and the approximate expression of Idc can be obtained as shown in formula (7):

$$i_{dc} = \frac{U_{dcN}}{wL_{eq}}e^{-\delta t}\sin(wt) - \frac{I_0 w_0}{w}e^{-\delta t}\sin(wt-\beta) \tag{7}$$

in the formula (7) are shown in formula (8):

$$\begin{cases} \delta = \dfrac{R_{line}+R_f}{2L_{eq}} \\ w = \sqrt{\dfrac{1}{C_{eq}L_{eq}} - \left(\dfrac{R_{line}+R_f}{2L_{eq}}\right)^2} \\ w_0 = \sqrt{\delta^2 + w^2} \\ \beta = \arctan\left(\dfrac{w}{\delta}\right) \end{cases} \tag{8}$$

After the converter station is locked, the transient fault will enter the fault isolation stage. At this time, the current path of MMC includes iCDSM>0 and iCDSM<0. The internal current path diagram of MMC is shown in Fig 5:

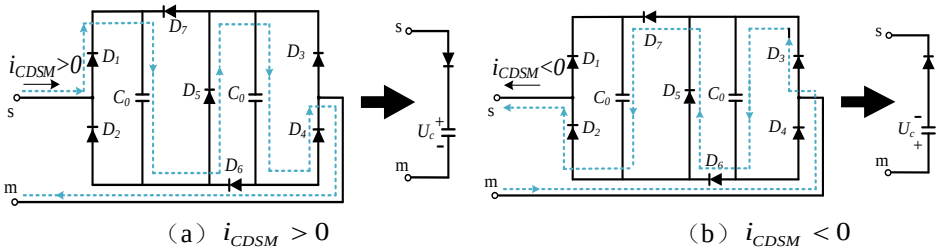

（a） $i_{CDSM} > 0$ （b） $i_{CDSM} < 0$

Figure 5: Internal current path diagram in fault isolation stage

As shown in Fig 5, series and parallel capacitors in the path will generate reverse potential in the fault loop, blocking the short circuit current. Due to the special structure of MMC, when entering the fault isolation stage, most of the stored energy in the AC/DC system will be returned to the capacitor, making its voltage rise, and the DC fault current will be reduced to zero.

C. DCT bipolar short-circuit fault characteristic analysis

Taking DAB, the submodule of DCT, as an example, fault characteristics are analyzed. Due to the electrical isolation effect of high-frequency transformer, when a bipolar short-circuit fault occurs in the DC line, the fault characteristics of the DC port are mainly affected by the circuit on the side near the fault point of the submodule. After the fault, the capacitance of the DC port will continue to discharge to the fault point, as shown by the dotted line in Fig 6:

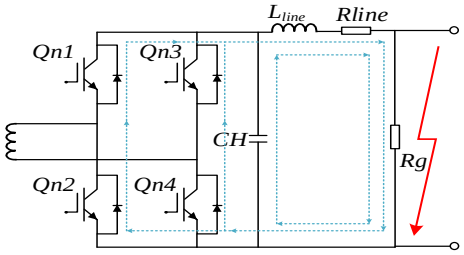

Figure 6: DAB fault circuit diagram

As shown in Fig 6, when the capacitor discharge ends, the fault current does not immediately drop to zero, but continues through the inductors and diodes in the circuit, during which the current gradually decreases until it drops to zero.

It can be seen that the discharge circuit of DAB is a second-order circuit discharge process, and the fault resistance in the DAB fault circuit is small, which is also a process of oscillation attenuation[21]. Therefore, when a bipolar short-circuit fault occurs at the high-voltage port of DCT, the fault current is shown as formula (10):

$$i_{dc} = \frac{U_{dcN}}{wL_{eq}} e^{-\delta t} \sin(wt) - \frac{I_0 w_0}{w} e^{-\delta t} \sin(wt - \beta) \tag{9}$$

Parameters in formula (10) are shown in formula (11) :

$$\begin{cases} L_{eq} = L_{line} \\ \delta = \dfrac{R_{line} + R_f}{L_{line}} \\ w = \sqrt{\dfrac{1}{C_H L_{line}} - \left(\dfrac{R_{line} + R_f}{2L_{line}} \right)^2} \\ w_0 = \sqrt{\delta^2 + w^2} \\ \beta = \arctan\left(\dfrac{w}{\delta} \right) \end{cases} \tag{10}$$

In the above formula, CH represents the capacitance value of the DCT near the fault side.

It can be seen from formula (7)-(10) that when the bipolar short-circuit fault occurs in the DC distribution network, the fault current expression at the outlet of MMC and DCT converters is a fixed value except for time.

To sum up, the time-domain forms of fault currents of MMC and DCT can be uniformly expressed as follows:

$$\begin{cases} \dfrac{U_{dcN}}{wL_{eq}} = A \\ \dfrac{I_0 w_0}{w} = B \end{cases} \tag{11}$$

$$i_{dc}(t) = Ae^{-\delta t} \sin(wt) - Be^{-\delta t} \sin(wt - \beta) \tag{12}$$

According to formulas (7) - (12), the time-frequency domain information of frequency-dependent attenuation is included in the current time-domain expression, where the attenuation coefficient δ is determined by the equivalent resistance and equivalent reactance of the fault loop, and δ is approximately proportional to the equivalent resistance Req and inversely proportional to the equivalent Leq.

III RESEARCH ON PROTECTION METHOD BASED ON PEAK-AVERAGE RATIO OF FAULT CURRENT ENERGY

A. Definition and characteristics of peak-to-average ratio of fault current energy

In this paper, the instantaneous energy of the current signal in formula (7) when the fault occurs is calculated by TEO. When the fault instant is $t = 0^+$, the formula (7) is differentiated once and twice to the time to obtain:

$$\frac{di_{dc}(t)}{dt} = \frac{U_{dc}}{L_{eq}} - \frac{R_S}{L_{eq}} I_0 \tag{13}$$

$$\frac{d^2 i_{dc}(t)}{dt^2} = -\frac{U_{dc} R_S}{L_{eq}^2} + (\frac{R^2{}_S}{L_{eq}^2} - \frac{1}{L_{eq} C_{eq}}) I_0 \tag{14}$$

In above formulas, RS is the equivalent resistance in the fault loop, that is, the sum of the transition resistance at the fault point and the equivalent resistance of the line. $\frac{di_{dc}(t)}{dt}$ is the first differential value of current to time, $\frac{d^2 i_{dc}(t)}{dt^2}$ is the second differential value of current to time, Udc is the rated value of DC voltage, Leq and Ceq are the equivalent values of inductance and capacitance of the fault loop respectively. I0 is the instantaneous value of the current at the protection installation point when the fault occurs.

Instantaneous energy of TEO calculated signal $x(t)$. $\psi[x(t)]$ is shown as follows[22] :

$$\psi[x(t)] = (\frac{dx(t)}{dt})^2 - x(t)\frac{dx^2(t)}{dt^2} \tag{15}$$

By bringing formulas (7), (13) and (14) into formula (15), the maximum instantaneous energy of fault current at the initial fault moment $\psi_{\max}$ can be obtained, as shown in formula (16):

$$\psi_{\max} = \frac{U_{dc}^2 C_{eq} - U_{dc} I_0 R_s C_{eq} + I_0^2 L_{eq}}{L_{eq}^2 C_{eq}} \tag{16}$$

Similarly, after a fault occurs, the instantaneous energy expression of the fault current is shown in formula (17) :

$$\psi = \frac{U_{dc}^2 C_{eq} - U_{dc} I_0 R_s C_{eq} + I_0^2 L_{eq}}{L_{eq}^2 C_{eq}} e^{-\frac{R_s}{L} t} \tag{17}$$

It can be seen that the maximum instantaneous energy of the fault current in formulas (16) and (17) $\psi_{\max}$ and the instantaneous energy value ψ at any time. decrease with the increase of the equivalent resistance RS of the fault loop, the larger the transition resistance, the smaller the instantaneous energy.

However, it is worth noting that when RS increases, the instantaneous energy value of the fault current will decay faster. Suppose that the average instantaneous energy value of the fault current within 1t after the fault occurs is t_1, then the approximate value of $\overline{\psi}$ is shown in formula (18) :

$$\overline{\psi} = \frac{U_{dc}^2 C_{eq} - U_{dc} I_0 R_s C_{eq} + I_0^2 L_{eq}}{L_{eq}^2 C_{eq}} (1 - e^{-\frac{R_s}{L_{eq}} t_1}) \cdot \frac{L_{eq}}{R_s t_1} \tag{18}$$

Then the ratio K of the maximum instantaneous fault energy $\psi_{\max}$ to the average instantaneous energy $\overline{\psi}$ is shown in formula (19) :

$$K = \frac{\psi_{\max}}{\overline{\psi}} = \frac{R_s}{L_{eq}} \frac{t_1}{(1 - e^{-\frac{R_s}{L_{eq}} t_1})} \tag{19}$$

It can be seen that the larger the RS, the smaller the $1 - e^{-\frac{R_s}{L_{eq}} t_1}$, the ratio K increases with the increase of the transition resistance. The ratio K of the maximum instantaneous fault energy $\psi_{\max}$ to the average instantaneous energy $\overline{\psi}$ is called the energy peak-average ratio.

Due to DC current is basically unchanged during normal operation of DC distribution network, the instantaneous energy value remains 0, it is necessary to appropriately add a small amount of bias value to the numerator and denominator of $K = \frac{\psi_{\max}}{\overline{\psi}}$ to keep the energy peak-average ratio K close to K=1 during normal operation of the system. Even if the system is disturbed by noise, $\psi_{\max}$ and $\overline{\psi}$ are both proportional to noise intensity. Theoretically, it is not affected by white noise and has strong anti-noise ability. When the energy peaking ratio K is applied to protection, only enough time window $t_1 > \frac{10 L_{eq}}{R_s}$ is selected to ensure $K >> 1$ in case of failure, which has a high protection margin and will not protect misoperation even in high noise environment.

a) Boundary characteristics of peak-to-average ratio of fault current energy

The equivalent inductance of a DC line is lower than that of its AC counterpart because it does not have the induction and capacitance effects caused by the continuously varying electromagnetic field of AC current, and the inductance of a typical overhead DC transmission line is probably in the range of 1 to 2mH/km, but this value varies depending on the specific design of the line[23]. The current limiting reactor's reactance value is generally 50mH. It can be seen that in a DC distribution system, the reactance value of the current limiting reactor is usually greater than that of a 25km line, so the presence of the current limiting reactor will significantly affect the energy peak-to-average ratio characteristics of the fault current. Fig 7 shows the fault current waveform when the bipolar short circuit fault occurs in the line outside the region, and the horizontal axis time scale "0" indicates the fault occurrence start time.

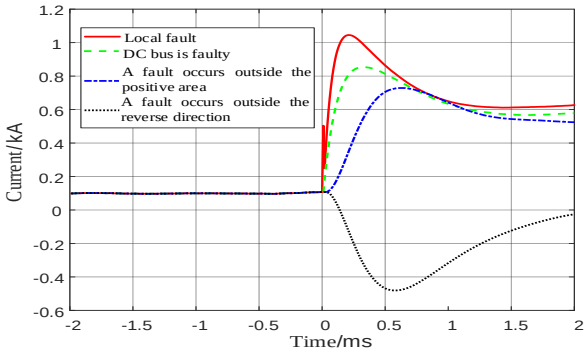

Figure 7: Waveforms of fault currents at different fault locations

As can be seen from Fig 7, the DC current basically remains unchanged before the 0ms fault occurs, and rises rapidly after the 0ms fault occurs. When the fault occurs, the current curve has a large mutation, and the degree of mutation caused by the fault at different positions is different. At the same time, when the fault occurs in different fault sections, the fault current waveforms are not only different in amplitude, but also significantly different in steepness.

It is easy to know that the reason for the above phenomenon is that the fault circuit needs to pass the current limiting reactor when the fault is outside the area, resulting in the total reactance Leq of the loop will be significantly higher than that of the fault in the area. Therefore, the energy peak-to-average ratio K value of the out-of-area fault will be significantly smaller than that of the in-area fault, and it can be seen that the faster the energy attenuation of the current waveform, the greater the energy peak-to-average ratio K value.

By converting the current curve into the current energy spectrum with TEO, the difference in current waveforms caused by different fault locations can be more intuitively analyzed. The fault current energy spectrum is shown in Fig 8:

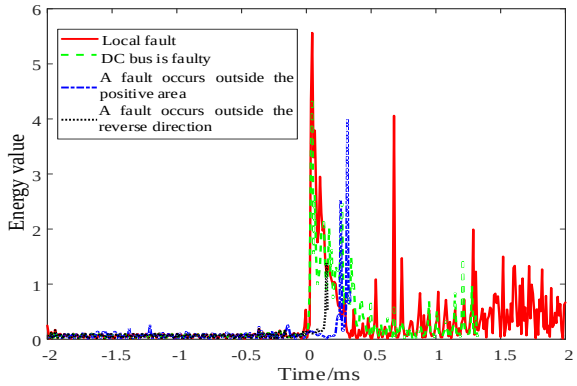

Figure 8: Fault current energy spectrum at different fault locations

As can be seen from Fig 8, the current energy of faults in the area is the largest, followed by the DC bus fault, and the current energy of faults outside the area is small. When approaching 2ms, the current energy of the above four fault conditions has decayed to almost the same, which means that the energy peak-to-average ratio of faults in the area will be greater than that of faults outside the area.

The calculated energy peak-to-average ratio K values of the above four faults are shown in Tab 1. The results are consistent with theoretical analysis, and the energy peak-to-average ratio of the faults within the region is obviously greater than that of the faults outside the region.

Tab 1 Energy peak-to-average ratio of faults at different locations

Fault	Fault location	Energy peak-average ratio
f1	Local fault	8.52
f2	The DC bus is faulty	6.96
f3	Out of area fault	6.61
f4	Out of area fault	6.25

b) Distance characteristics of peak -average ratio of fault current energy

According to formula (20), the peak-to-average ratio of fault current energy increases with the increase of fault loop resistance, the farther the fault point is from the power supply, the greater the peak-to-average ratio of fault energy. However, the equivalent resistance value of flexible DC distribution lines is usually between 0.07 and 0.1 ohms/km[24]. Therefore, the influence of fault distance on peak-to-average ratio of fault current energy is relatively small in theory.

Fig 9 shows the fault current waveform diagram at different distances, which well confirms the above theoretical analysis.

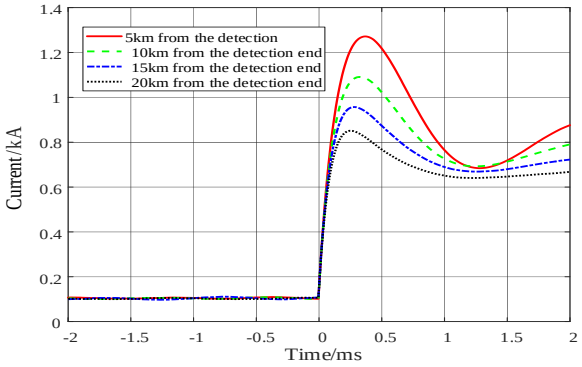

Figure 9: Waveform diagram of fault current at different fault distances

The current waveform in Fig 9 cannot visually detect the fault current attenuation at different fault distances. By converting the current curve into the current energy spectrum with TEO, the fault energy characteristics at different fault distances can be more intuitively analyzed, as shown in Fig 10:

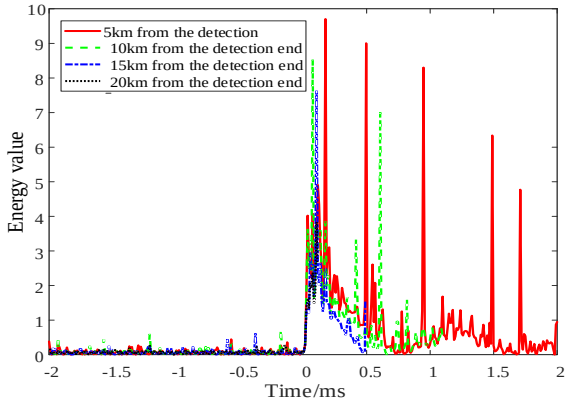

Figure 10: Fault current energy spectrum at different fault distances

As shown in Fig 10, it can be seen that the current energy after the fault occurs is $X1>X2>X3>X4$, but the difference is not much. When approaching the 2ms, the current energy is still $X1>X2>X3>X4$, and the relative gap is larger, that is, the farther the fault distance is, the faster the energy decay rate is, which means that the energy peak-average ratio increases with the increase of the fault distance.

The calculated energy peak-average ratio K values of the above four faults are shown in Tab 2, and the results are consistent with theoretical analysis. The longer the fault distance is, the larger the energy peak-average ratio will be. Moreover, since the resistance value of DC distribution lines is not high, the fault distance has relatively little influence on the energy peak-average ratio.

Tab 2 Energy peak-to-average ratio at different fault distances

Fault	Fault distance	Energy peak-average ratio
x1	5km	8.32
x2	10km	8.56
x3	15km	8.77
x4	20km	8.94

B. Protection method combining current abrupt change and energy peak-average ratio

The current mutation $\frac{di_{dc}(t)}{dt}$ in formula (13) decreases with the increase of loop resistance RS and decreases with the increase of equivalent reactance Leq. The equivalent reactance Leq increases due to the presence of a current-limiting reactor in the out-of-area fault, and the current mutation will be smaller than that in the in-area fault. Fig 11 shows the fault current waveforms under different conditions inside and outside the region.

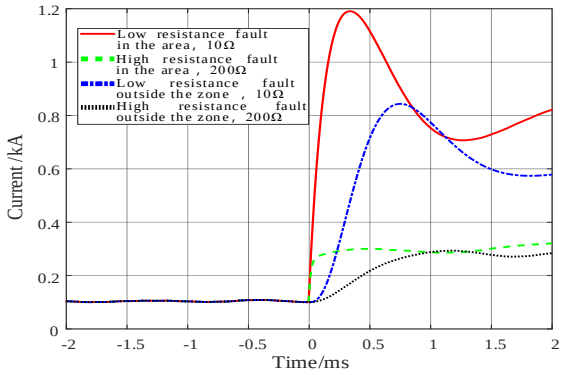

Figure 11: Fault current waveform of different fault conditions

As can be seen from Fig 11, the current mutation of faults within the region is relatively severe, while that of faults outside the region is relatively gentle, and the current amplitude of faults with low resistance is significantly greater than that of faults with high resistance.

The expression of current sudden change is shown in formula (20):

$$\frac{\Delta i_{dc}(n)}{\Delta t} = \frac{i_{dc}(n) - i_{dc}(n-1)}{\Delta t} \tag{20}$$

In above formula, $i_{dc}(n)$ is the DC current signal collected at the sampling point, Δt is the sampling interval, which is 0.01ms in this paper.

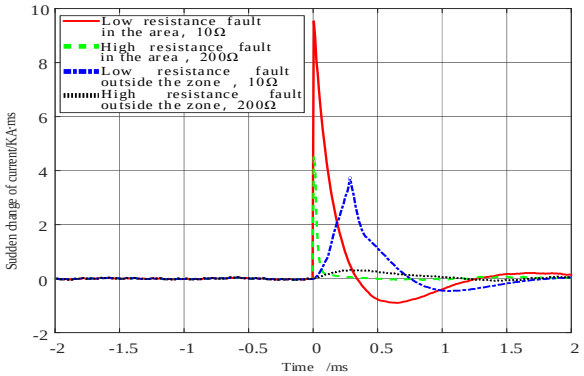

Figure 12: Abrupt change of fault currents under different fault conditions

The formula (20) is used to calculate the current waveform in Fig 11, and the current abrupt changes in different fault conditions can be obtained as shown in Fig 12. The maximum current abrupt changes in the four fault conditions in Fig 12 are shown in Tab 3:

Tab 3 The maximum value of current abrupt change under different fault conditions

Fault	Fault condition	The maximum value of current sudden
y1	Low resistance fault in the area (10km,10Ω)	9.53 kA·ms
y2	High resistance fault in the area (10km,200Ω)	4.59 kA·ms
y3	Low resistance fault outside the zone (35km,10Ω)	3.77 kA·ms
y4	High resistance fault outside the zone(35km,200Ω)	0.32 kA·ms

It can be seen from Fig 12 and Tab 3 that the current mutation amount of faults within the region is greater than that of faults outside the region, and the current mutation amount of faults with low resistance is greater than that of faults with high resistance. However, it is worth noting that the current sudden change is difficult to distinguish between high-resistance faults in the area and low-resistance faults outside the area.

In order to solve the above situation, this paper further explores the changes of energy peak-to-average ratio and current mutation under different fault distances and transition resistances, as shown in the fig below.

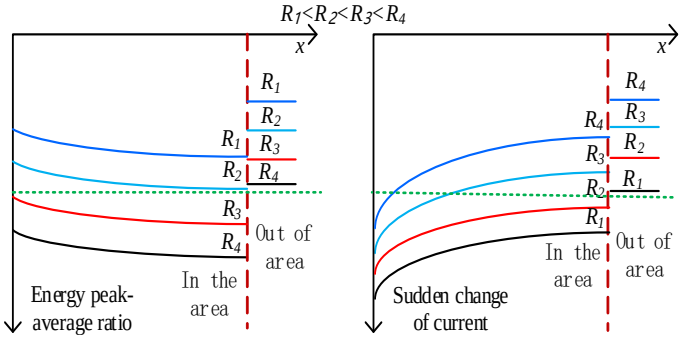

Figure 13: Schematic diagram of the change law of energy peak-to-average ratio and current mutation

As can be seen from Fig 13, if the characteristic value represented by the green dashed line in the fig is taken as the protection criterion, then the energy peek-to-average protection can correctly identify the faults of all lines in the region when the transition resistance is R3, R4 and higher, and the current mutation can correctly identify the faults of all lines in the region when the transition resistance is R1, R2 and lower.

In summary, the current abrupt change magnitude has the following characteristics: the current abrupt change quantity of low resistance faults in the region is much larger than that of high resistance faults in the region and high and low resistance faults outside the region. The energy peak-to-average ratio K has the following characteristics: The energy peak-average ratio K value under the high resistance fault in the region is greater than the K value under the low resistance fault in the region and the high and low resistance fault outside the region. In other words, the current sudden change is easier to identify the low resistance fault in the region, and the energy peak is easier to identify the high resistance fault in the region, and the two characteristics have strong complementarity.

Therefore, based on the above derivation and analysis of the energy characteristics of the current waveform, this paper proposes a protection method combining the energy peak-average ratio and the current mutation, and realizes the single-end instantaneous protection for the full length of the line through the complementary characteristics of the energy peak-average ratio and the current mutation.

C. Setting method for bipolar short-circuit fault protection

The protection scheme proposed in this paper is based on the protection of low resistance fault by the current mutation, and the protection of high resistance fault by the energy peak. The setting values of the energy peak-average ratio and the current mutation need to form coordination to achieve the overall protection effect. The protection setting method is as follows:

(1) Protection setting scheme based on current sudden change

After the protection is started, the current sudden change in the 1ms time window is used for preliminary judgment, and two setting values need to be set to cooperate with the peak-to-average energy protection. The $\lambda_{\max}$ is a fixed value, which is used to complete the protection determination directly by the current sudden change under the condition of low resistance fault; the $\lambda_{\min}$ is an adaptive value. When the sudden change of fault current is between two setting values, a fault can be determined. However, it is impossible to identify whether the fault occurs within

or outside the region only by the sudden change of current as the protection criterion, so it is necessary to start the peak-to-average energy ratio algorithm.

In this paper, the maximum value of protection setting is taken as the case of the maximum out-of-area current mutation (metal fault of the bus)[25], as shown in formula (21) :

$$\lambda_{\max} = K_{rel1} \frac{U_{dc}}{L_{eq} + L_{dc}} \tag{21}$$

In above formula, Udc is the DC voltage during normal operation, Leq is the equivalent reactance of the full length of the line, Ldc is the reactance value of the current-limiting reactor, and Krel1 is the reliability coefficient, which generally ranges from 1.1 to 1.3[26], and is 1.2 in this paper. Because the length of the distribution line is usually short, the equivalent reactance Leq of the line is smaller than that of the current limiting reactor Ldc, so the setting value can realize the full line quick action protection under the premise of ensuring the protection does not misoperate.

In this paper, the minimum setting value of current sudden change is set in the case of high-resistance fault (200Ω), and the calculation is shown in formula (22) :

$$\lambda_{\min} = \frac{U_{dc}}{L_{eq}} - \frac{200}{L_{eq}} I_0 \tag{22}$$

In above formula, I0 is the load current during normal operation.

(2) Protection setting scheme based on current energy peak-to-average ratio

Because the peak-to-average ratio of fault current energy increases with the increase of transition resistance, the peak-to-average ratio of current energy for out-of-area faults is significantly smaller than that for in-area faults. Therefore, the peak-to-average energy ratio of the high-resistance fault outside the area is close to that of the low-resistance fault inside the area. When the fault with the highest peak-to-average energy ratio outside the area - the busbar high-resistance fault (200Ω) is used[27], the detected energy peak-to-average ratio of 0K is set as the threshold, as shown in formula (23) :

$$K_{\max} . . K_{set} = K_{rel2} K_0 \tag{23}$$

In above formula, Kmax is the maximum energy peak-to-average ratio in the 1ms time window after the fault occurs, and Krel2 is the reliability coefficient. Since the peak-to-average ratio of energy is less affected by noise and is not easy to mismove, the value of Krel2 in this paper is 1.1.

IV SIMULATION EXPERIMENT VERIFICATION

To verify the reliability of the proposed protection under various fault conditions, a ±10kV multi-terminal circular flexible DC distribution network model was built in PSCAD/EMTDC, as shown in Fig 1.

The sampling rate is set to 100kHZ, and the DC circuit breaker at the 1lM end of the line in Fig 1 is used as the simulation test object.

As the DC distribution network contains a large number of power electronic components, their equivalent resistance and equivalent reactance are difficult to determine accurately, so the setting values of each criterion are determined by simulation in this paper, as shown in Tab 4:

Tab 4 sets the values of each criterion

criterion	Setting value
Protection start criteria	mset=10kV·ms
Fault direction identification criterion	εset=0.05kA·ms
Ground fault identification criteria	nset=0.5kV·ms
Current abrupt change criterion	$\lambda_{\max}$ =5kA·ms $\lambda_{\min}$ =0.05kA·ms
Energy peak-average ratio criterion	K_{set} =8

A. Reliability Verification of Protection methods

In order to verify that the proposed method can protect the whole length of the area and avoid misoperation when the fault occurs outside the area, several extreme fault situations are set up for simulation verification, and the faults

all occur at the 2ms. Where, set the fault f1 in the area, the bus fault f2, and the fault f3 outside the area corresponding to the position marked in Fig 1, and use the fault type as shown in formula (24) to mark:

$$f_a|(x, R_f) \tag{24}$$

In above formula, a represents the fault location, x represents the fault distance, and Rf represents the transition resistance.

The faults are f1|(1km, 0Ω) at the near end of the zone, f1|(24km, 200Ω) at the far end of the zone, f2|(25km, 0Ω) at the bus bar, f2|(25km, 200Ω) at the bus bar, and f3|(30km, 30km, 200ω) at the outside of the zone. High resistance fault outside the f3 area f3|(30km, 200Ω). The fault current waveform is shown in Fig 14:

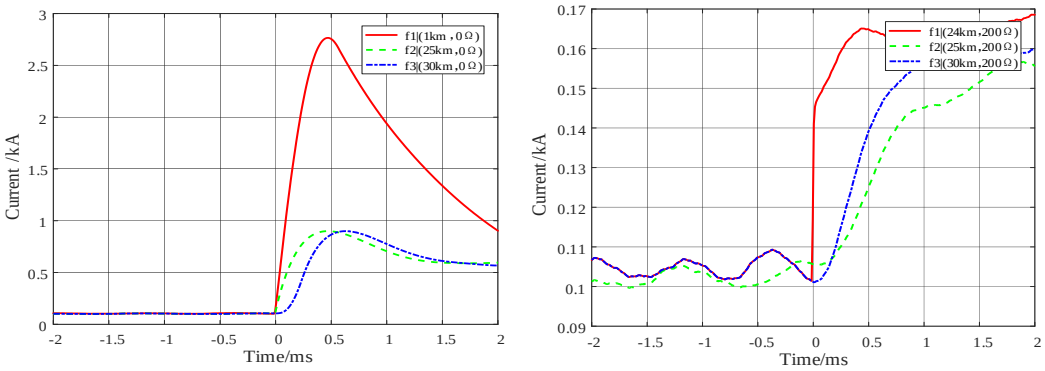

(a) (b)

Figure 14: Fault current waveform under extreme conditions

According to the fault current waveform signal shown in Fig 14, the corresponding current mutation amount and energy peak-to-average ratio are calculated. The current mutation amount changes are shown in Fig 15:

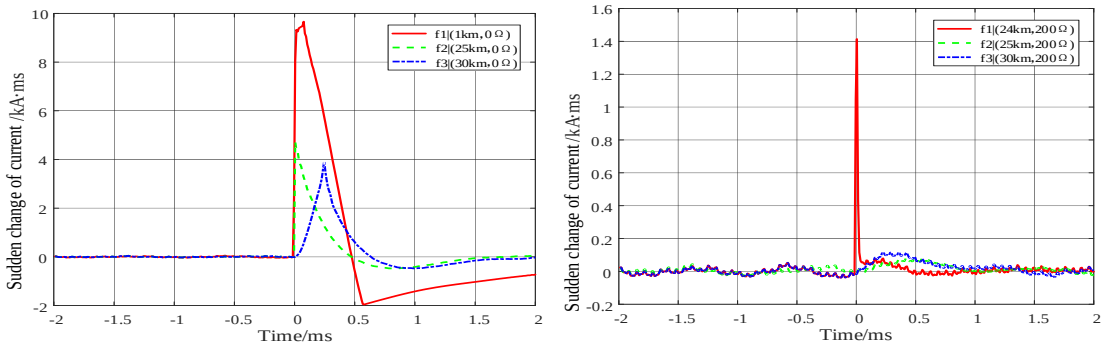

(a) (b)

Figure 15: Sudden change of current in extreme cases

As can be seen from Fig 15, the characteristics of the current mutation quantity are obvious in the case of low-resistance faults, and the faults inside and outside the region can be distinguished significantly by relying on the current-limiting reactor as the line boundary. However, the fault characteristic quantity is seriously affected by the transition resistance, and the fault identification can only be carried out by relying on the energy peaking to average ratio introduced as the fault characteristic quantity in the case of high-resistance faults.

Tab 5 Fault identification in extreme cases

Fault	The maximum value of current sudden /kA·ms	Energy peak-average ratio	Result
f1(1km,0Ω)	9.66	7.13	Local fault
f1|(24km,200Ω)	1.41	10.69	Local fault
f2|(25km,0Ω)	4.72	6.62	Out of area fault
f2|(25km,200Ω)	0.13	7.57	Out of area fault
f3|(30km,0Ω)	3.92	6.36	Out of area fault
f3|(30km,200Ω)	0.09	6.86	Out of area fault

In combination with Tab 5, it can be seen that only the current sudden change criterion can accurately identify faults in the area when the transition resistance is very small, and only the energy peak-to-average ratio criterion can accurately identify faults in the area when the transition resistance is very large. The setting values of the two fault characteristics cooperate with each other, which can realize the single-end instantaneous quick protection against 0-200Ω bipolar short circuit fault of the full length of the line.

B. Anti-interference capability verification

Since the actual DC distribution network faults may be accompanied by a large amount of noise[28], this paper verifies the fault identification reliability of the proposed method under noisy conditions by adding Gaussian white noise to the simulation. Add 30db noise to the 6 groups of fault current waveforms in Fig 15 respectively, as shown in Fig 16:

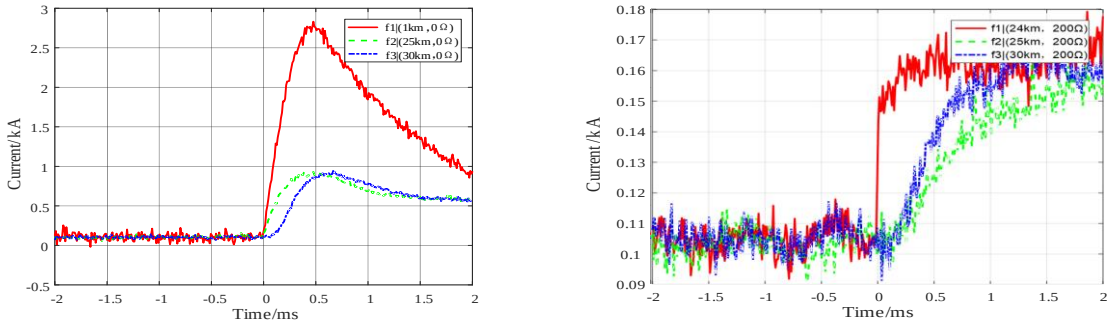

（a） （b）

Figure 16: Fault current waveform with noise

As can be seen from Fig 16, in the case of high-resistance faults, the fault current is greatly affected by noise, and the fault transient information has the risk of being submerged by noise. In this case, the energy peak-to-average ratio is used to determine the fault.

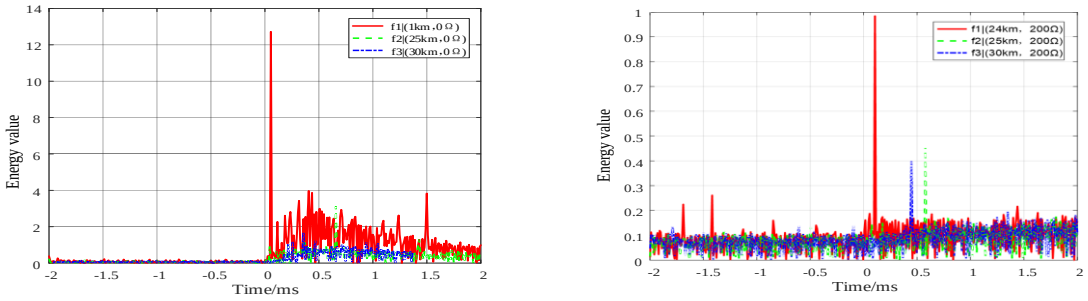

（a） （b）

Figure 17: Energy diagram of fault current with noise

As can be seen from Fig 17, after the fault current waveform is calculated by TEO, the obtained fault current energy diagram not only greatly reduces the noise interference, but also amplifies the fault transient information, which makes the proposed method have strong anti-noise ability.

The fault identification in the case of noise is shown in Tab 6:

Tab 6 Fault identification under noise condition

Fault	The maximum value of current sudden /kA·ms	Energy peak-average ratio	Fault identification result
f1|(1km,0Ω)	10.26	7.12	Local fault
f1|(24km,200Ω)	2.11	9.06	Local fault
f2|(25km,0Ω)	4.87	5.73	Out of area fault
f2|(25km,200Ω)	1.78	6.48	Out of area fault
f3|(30km,0Ω)	4.19	3.43	Out of area fault
f3|(30km,200Ω)	1.50	4.45	Out of area fault

By comparing Tab 5 with Tab 6, it can be seen that the current sudden change greatly under noisy conditions. The maximum current sudden change value under fault f2|(25km, 0Ω) is already close to the maximum setting value. Therefore, for high-noise lines, the anti-noise ability can be enhanced by increasing the setting value of the current sudden change criterion. At the same time, it can be seen that the energy peak average is less affected by noise, and the protection will not be misactivated due to noise interference, and it has a good anti-noise ability.

In practical engineering applications, the sampling frequency of DC protection is generally 10kHZ or 100kHZ, and the sampling rate designed in this paper is 100kHZ, and the data window length of 1ms is used for protection calculation. With the current speed of FPGA technology, the protection calculation time does not exceed 0.3ms. Since the length of a single distribution line is usually not more than 30km, the line transmission delay of the fault electrical wave is not more than 0.1ms, and the protection start delay is generally 15μs, the proposed protection method can operate within 1.5ms after the fault occurs. Meet the requirements of instantaneous quick action within 3ms of DC protection.

V SUMMARIZE

Based on the fact that traditional flexible DC distribution network fault protection methods cannot judge faults and line protection problems in a very short time, this paper analyzes the bipolar short-circuit fault characteristics, explores the complementary relationship between current mutation and energy peak-average ratio, and thus forms a protection method combining current mutation and energy peak-average ratio, and draws the following conclusions:

(1) The characteristics of bipolar short-circuit fault are deeply explored in this paper. The transient discharge process of bipolar short-circuit fault is derived theoretically, and the unified expression form of bipolar short-circuit fault current in time domain of flexible DC distribution network is obtained, and the waveform characteristics of fault current in DC distribution network are revealed.

(2) A protection method combining current mutation and energy peak-to-average ratio is proposed. This paper first defined the energy peak-average ratio, and then explored the complementary characteristics between the current mutation and the energy peak-to-average ratio, revealing the law that the current mutation can accurately identify faults inside and outside the region, and the energy peak-to-average ratio can accurately identify high-low resistance faults. Therefore, this paper realized the single-end instantaneous protection for the full length of the line through the complementary characteristics of the two.

(3) The protection method proposed in this paper is not affected by the fault location, transition resistance and strong noise, and solves the problem that the traditional single-end protection cannot operate correctly when the fault is high resistance or large noise.

(4) The protection method proposed in this paper has a fast action speed. When the sampling frequency of the protection device is 100kHZ, it can act quickly within 1.5ms after the fault occurs, and meet the fast action requirements of the flexible DC distribution network protection within 3ms.

VI ACKNOWLEDGMENT

This work was supported by China Southern Power Grid Digital Power Grid Group Co., Ltd. This work was funded by the project of China Southern Power Grid Digital Power Grid Group Co., Ltd. (Number: 210002KK52222011).

REFERENCES

[1] Qi, H., Chen, W., Dou, Z., Han, J., Sun, P., Zhang, Z., & Yin, X. (2023). Fault Characteristic Analysis and a Novel Pilot Protection Scheme for Pole-to-Ground Fault in Flexible DC Distribution Network. IEEE Access, 11, 74071–74087.

[2] Qi, Z. (2023). Operation control method of relay protection in flexible DC distribution network compatible with distributed power supply. Energy Engineering, 120(11), 2547-2563.

[3] Wang, H., Zhou, N., Zhang, Y., Liao, J., Tan, S., Liu, X., Guo, C., & Wang, Q. (2024). Linearized power flow calculation of bipolar DC distribution network with multiple flexible equipment. International Journal of Electrical Power and Energy Systems, 155.

[4] Wang, C., Li, P., Xu, X., & Gao, H. (2022). A DC Fault Location Method of Multiterminal Flexible DC Distribution Network. Mathematical Problems in Engineering, 2022.

[5] Ma, T., Hu, Z., Xu, Y., & Dong, H. (2022). Fault Location Based on Comprehensive Grey Correlation Degree Analysis for Flexible DC Distribution Network. Energies, 15(20).

[6] Wang, D., Wang, B., Zhang, W., Zhang, C., & Yu, J. (2021). Fault Location with High Precision of Flexible DC Distribution System Using Wavelet Transform and Convolution Neural Network. Frontiers in Energy Research, 9.

[7] Lobaton, P. G. O., Magtiay, J. E. C., Mendez, V. G. E., Moster, G. J. G., Casabuena, M. M., Gaspar, M. M., & Mojares, P. V. (2024). LEAFLET: A Web-Based Leaf Classification System Using Convolutional Neural Networks. Journal of Electrical Systems, 20(1), 18–32.

[8] Wei, Y., Wang, Z., Liu, K.-Z., Wang, P., Zeng, Z., & Wang, X. (2022). Fault detection method of flexible DC distribution network based on color relation analysis classifier. Electrical Engineering, 104(6), 4543–4556.

[9] Rui L, Lie X, Liangzhong Y. DC Fault Detection and Location in Meshed Multiterminal HVDC Systems Based on DC Reactor Voltage Change Rate [J]. IEEE Transactions on Power Delivery, 2017,32(3):1516-1526.

[10] Diao, X., Liu, F., Song, Y., Xu, M., Zhuang, Y., & Zha, X. (2021). An Integral Fault Location Algorithm Based on a Modified T-Source Circuit Breaker for Flexible DC Distribution Networks. IEEE Transactions on Power Delivery, 36(5), 2861–2871.

[11] Nidhyananthan, S. S., Suganya, R., Kiruba, S., Suganya, D., Rangaree, P., Biswas, P., & Roy, B. (2024). Impact of Intense Modulation on Soliton Power Propagation across Optical Fiber and Optical Wireless Channels. Journal of Electrical Systems, 20(1), 362–368.

[12] Sathish, C. H., Chidambaram, I. A., & Manikandan, M. (2023). Switched Z-Source Boost Converter in Hybrid Renewable Energy System for Grid-Tied Applications. Journal of Electrical Systems, 19(1), 64–81.

[13] Dai, Z., Liu, S., Chen, S., Zhao, J., & Wu, T. (2022). Flexible DC distribution line protection principle based on distance metric of clustering centres. IET Generation, Transmission and Distribution, 16(18), 3661–3672.

[14] Zheng, T., Lv, W., Wu, Q., Li, R., Liu, X., Zhang, C., & Xu, L. (2021). An Integrated Control and Protection Scheme Based on FBSM-MMC Active Current Limiting Strategy for DC Distribution Network. IEEE Journal of Emerging and Selected Topics in Power Electronics, 9(3), 2632–2642.

[15] Zheng, F., Zhang, J., Lin, J., Deng, C., & Huang, J. (2022). A Novel Flexible Fault Current Limiter for DC Distribution Applications. IEEE Transactions on Smart Grid, 13(2), 1049–1060.

[16] Jia, K., Feng, T., Wang, C., Zhu, R., & Bi, T. (2020). Current Ratio Based Breakage Protection for Flexible DC Distribution Systems. IEEE Transactions on Power Delivery, 35(5), 2300–2309.

[17] Dai, Z., Liu, X., He, Y., & Huang, M. (2020). Single-Terminal quantity based line protection for ring flexible dc distribution grids. IEEE Transactions on Power Delivery, 35(1), 310–323.

[18] Jin, W., Wang, Z., Wang, H., Feng, S., & Liang, R. (2024). A novel fault section location method for single pole to ground fault of DC distribution lines. IET Renewable Power Generation, 18(7), 1394–1405.

[19] Jamshidifar, Aliakbar, Jovcic, et al. Small-Signal Dynamic DQ Model of Modular Multilevel Converter for System Studies [J]. IEEE Transactions on Power Delivery, 2016, 31 (1): 191-199.

[20] Xu, X., Huang, W., Hu, Y., Tai, N., Ji, Y., & Xie, N. (2021). Power Management of AC/DC Hybrid Distribution Network With Multi-Port PET Considering Reliability of Power Supply System. Frontiers in Energy Research, 9.

[21] Zihan Q. Operation Control Method of Relay Protection in Flexible DC Distribution Network Compatible with Distributed Power Supply [J]. School of Electric Power Engineering, South China University of Technology , Guangzhou, 510641 , China, 2023, 120 (11): 2547-2563.

[22] Chen S. Line fault location of flexible DC distribution network based on adaptive noise empirical mode decomposition [J]. Journal of Physics: Conference Series, 2024, 2683 (1):

[23] Jia, K., Xuan, Z., Feng, T., Wang, C., Bi, T., & Thomas, D. W. P. (2020). Transient high-frequency impedance comparison-based protection for flexible DC distribution systems. IEEE Transactions on Smart Grid, 11(1), 323–333.

[24] Yuan, S., Yan, J., Yu, Y., Zhao, C., Su, G., & Li, X. (2022). Calculation method of short-circuit fault current in flexible DC grid. Energy Reports, 8, 461–468.

[25] Zhang, J., Gao, Y., Xiao, F., Guo, F., Li, X., Han, Y., & Li, L. (2019). Study on DC breaker fault current and its limiting method of multiterminal flexible DC distribution system. Energies, 12(5).

[26] Dhanalakshmi, K. V., Panigrahi, P. K., & Kumar, G. R. (2023). Fault Analysis of Microgrid With Grid-Connected and Islanded mode Using IoT-Wavelet Approach. Journal of Electrical Systems, 19(1), 13–26.

[27] Jiang, L., Yin, X., Lai, J., Chen, W., Wen, M., Dou, Z., Fang, J., & Xiong, Z. (2024). A novel voltage arc suppression method for single-phase grounding fault in distribution network based on power router. Electric Power Systems Research, 231.

[28] Guo, P., Tian, Z., Yuan, Z., Zhang, X.-Y., & Sharifi, D. (2024). Research on Symmetric Bipolar MMC-M2Tdc-Based Flexible Railway Traction Power Supply System. IEEE Transactions on Transportation Electrification, 10(1), 1043–1055.